International Journal of Multiphase Flow 169 (2023) 104602

Contents lists available at ScienceDirect

International Journal of Multiphase Flow

journal homepage: www.elsevier.com/locate/ijmulflow

The pairwise interaction of coalescing air bubbles in water

Mustapha A. Al-Behadili [a,b,c,*], David M. Hargreaves [a], Buddhika N. Hewakandamby [a]

[a] Faculty of Engineering, University of Nottingham, NG7 2RD, UK
[b] Petroleum Engineering Department, Al-Amarah University College, Maysan, 62001, Iraq
[c] Missan Oil Company, Maysan, 62001, Iraq

ARTICLE INFO

Keywords:
Bubble dynamics
Bubbly flow
Coalescence
Wakes
CFD
Adaptive mesh

ABSTRACT

There is a relative scarcity of experimental data relating to the interaction of a pair of millimetre-scale air bubbles rising having an offset configuration through stagnant water. To add to this dataset was the motivation behind this work. A series of experiments are presented, which can add to the understanding of bubble-bubble interaction. The trajectories of bubble pairs were tracked using a high speed camera. The diameter and relative positions of the nozzles were varied to produce different separation distances between the rising bubbles. It was found that when the trailing bubble is slightly smaller (as little as 2.3%) than the leading bubble it would approach the leading bubble. Hence, a greater tendency to coalesce between the rising pairs has been noticed. The initial relative angle between the coalesced bubbles, θ_i, was also correlated which has agreed well with others' previous work. A proportional relationship has been presented to link the time required for coalescence with the ratio of the bubbles radii. A complementary set of numerical simulations, using a multiphase CFD model with adaptive meshing, have confirmed some of the experimental observations and added insights into the flow structures responsible for coalescence. Finally, a map for the boundaries of coalescence from the numerical and experimental observations is suggested which relates the separation of the bubbles and their radii ratio to the likelihood of coalescence.

1. Introduction

Many industrial chemical processes involve bubbles dispersed in liquid flows. Bubbly flows contain large numbers of bubbles in close proximity. Such flows are complex due to the interactions among the bubbles. Processes such as coalescence, bouncing and wake interactions behind rising bubbles all influence the structure of bubbly flow. Therefore, accurate modelling of bubbly flow requires an approach that accounts for bubble-bubble interaction. Single bubble models do not cater for pairwise interaction, so an approach that includes this effect is a better, more complete approach to modelling because it assumes bubbles affect each other (Magnaudet and Eames, 2000).

The interaction of a pair of bubbles rising has been the subject of many investigations, (Harper, 1970; Biesheuvel and Van Wijngaarden, 1982; Kumaran and Koch, 1993a,b; Van Wijngaarden, 1993; Ruzicka, 2000). The majority of these studies have been numerical or analytical. Spherical bubbles having the same radius, r, less than 1 mm are assumed to rise at low or moderate Reynolds numbers. For a range of Reynolds number, Re ~ 500, Kok (1993a) solved the viscous drag force for a pair of spherical bubbles using potential flow theory. For bubbles rising with an initial relative angle, θ_i, the angle between the bubbles' centerline and the horizontal axis, he pointed out that the bubbles attract each other when θ_i is between 35° and 54.7°. His solution of inviscid flow theory predicted that the trailing bubble had higher drag than the leading one. A similar result was also reported by Harper (1970). The Direct Numerical Simulations (DNS) of Yuan and Prosperetti (1994), however, for spherical bubbles rising in-line showed the opposite situation where the trailing bubble experienced less drag. That was due to the flow field generated by the upward passage of the leading bubble. They also pointed out that the balance between the repulsive and the attractive forces in the wake led the bubbles to maintain an equilibrium distance between each other. Their pioneering work established a solid ground for further progress in bubble-bubble interaction studies. Their finding about this equilibrium distance was supported experimentally by Watanabe and Sanada (2006) for intermediate Reynolds number, $5 < \mathrm{Re} < 150$, albeit large differences were observed between the theory and the experiments. However, for low Reynolds number, that equilibrium distance was not observed in the experiments of Katz and Meneveau (1996). The existence of the equilibrium distance was, however, confirmed by the DNS work of Legendre et al. (2003) for two bubbles rising side by side. It has been recently shown that the case in which the bubbles rising in line is not stable and difficult to be achieved in real situation after the numerical simulations of Hallez and

* Corresponding author at: Faculty of Engineering, University of Nottingham, NG7 2RD, UK.
E-mail address: mustafa.abbas@alamarahuc.edu.iq (M.A. Al-Behadili).

https://doi.org/10.1016/j.ijmultiphaseflow.2023.104602
Received 2 April 2023; Received in revised form 6 July 2023; Accepted 25 August 2023
Available online 27 August 2023

Legendre (2011). This is because they found that the lift force induced by the vorticity of the leading bubble wake causes the lateral migration of the trailing bubble away from the path of the leading bubble. The magnitude of fluctuations in velocity that the vorticity produce when the bubbles rise side by side was studied by Van Wijngaarden (2005).

Vast body of the research on the pairwise interaction of bubbles has been done on bubbles rising in line or side by side (Balla et al., 2020). While, bubbles rising at infinite configuration, bubbles having offset, few studies have been carried out. For example, Hallez and Legendre (2011) derived the drag and lift coefficients for each bubble. Moreover, they described the interaction between the bubbles in terms of three factors. These are: potential effects; viscous correction or (Moore, 1963) correction; and the influence of the wake when one bubble is located in the wake of another. Baz-Rodríguez et al. (2014) proposed relating the trailing bubble with the flow structure of wake of the leading bubble for bubbles rising in-line by analytical approximation model based on the axial velocity in the wake. From the experimental perspective, the boundaries between coalescence and bouncing of two bubbles have been studied by many researchers. Duineveld studied the behaviour of two bubbles of different sizes as they encounter each other (Duineveld, 1995, 1998). In the 1998 paper, for instance, he investigated dual bubbles with radii up to 2 mm, released at different positions (side by side or in-line configurations). He observed that there is a critical Weber number that controls bouncing or coalescing of bubbles. In his work, the horizontal velocity was suggested as the characteristic velocity for the criteria of defining the Weber and Reynolds numbers. Similarly, Lehr et al. (2002) found that large and small relative velocities as the bubble approached each other resulted in bubble bouncing and coalescence, respectively. On the other hand, Sanada et al. (2009) studied the conditions at which the bubbles coalesce or bounce in terms of dimensionless numbers Reynolds and Weber for bubbles rising side by side. They suggested that the vertical rise velocity of the bubble is better than the horizontal velocity in defining Re and We. Recently, Kusuno and Sanada (2015a) investigated the rise of clean spherical air bubbles, $0.274 < r < 0.563$ mm, in line motion. Their results showed that the growing lift force of the wake results in the trailing bubble deviating from the vertical position causing a relative motion between the bubbles. Based on that, the pair of bubbles showed four types of motions: approaching, separating, coalescing and overtaking. It was concluded that those types were a function of their initial radius ratio (trailing bubble radius to leading bubble radius) even though they were at an appreciable small deviation (1%) since the larger bubble has generally the higher rise velocity. They reported that the bubbles attracted and collided to each other only when the trailing bubble approached the leading bubble from the side. For contaminated water, the bubbles collided at 90° (Kusuno and Sanada, 2015b). Recent studies have been focused on entering the boundary scales between the bubbles and constructing flow maps for the bubble-bubble interaction or coalescence. For example, Agrawal et al. (2021) have studied the interaction between a pair of identical bubbles rising side by side. They found that the bubbles are not affecting each other if the separation distance between their centres is greater than seven times the bubble radius. While, Balla et al. (2021) have introduced a regime map that demarcating the repulsive and attractive boundaries between two non coalescing gas bubbles rising side by side in a non-isothermal self-rewetting fluid. A very recent study has been done by Zhao et al. (2022) on establishing a regime map for the bubble departure induced by coalescence. They have identified four regions in that map in relation to the contact angles. It is noticeable here that the experimental evidence covers only a very small part of the parameter space studying the motion of bubbles at high Reynolds numbers, for example, Re ∼ 950. The objective of this paper is to shed light on the interaction between two bubbles, at the millimetre-scale, rising, and possibly coalescing, in close proximity. Section 2 describes both the experimental setup and numerical modelling, while Section 3 details the experimental findings of interaction of bubble pairs at small separation distances. Section 4 then shows the numerical results and compares them with the experimental observations, while Section 5 summarises and critiques our findings.

2. Experimental setup and numerical method

2.1. Experimental setup and procedure

An experimental rig was built to investigate the pairwise interaction of bubbles. A rectangular box was fabricated with a cross section of 100×100 mm which was large enough to eliminate wall effects on the bubbles. The height of the box was 500 mm. The generation of dual bubbles was achieved by placing two stainless steel nozzles side by side at the centre of the box. The nozzles were fixed into a brass base that was designed so that the nozzles to be removed independently in such a way that many axial separation, Δx, and as a result different centre to centre separation, s, between the bubbles could be achieved. The internal diameter of each nozzle, D_i, is 2 mm which produced bubbles at about 2 mm equivalent radius, r. The air is pumped through each nozzle using a separate syringe pump of the same model with a low flowrate to reduce background perturbations induced by the wakes of a rising series of bubbles.

Depending on the timing of the release, two bubbles with appreciable deviation in radii can be generated. The leading bubble, B_1 – by definition the first generated bubble (although it may come from either nozzle) – on occasion, assumes an ellipsoidal shape even before the second bubble, B_2, trailing bubble, is released.

Tap water was used here as a liquid phase and was allowed to become still before each experiment. The experiments were carried out at room temperature ($\approx 21\ ^\circ C$) and at atmospheric pressure. In order to track the interaction between the bubbles in three dimensions, a mirror having the same specifications of that was previously used by Lunde and Perkins (1998) was used here.

The mirror (220 mm×60 mm) was positioned at an angle of 45° to the centreline of the camera outside the rig. Therefore, two planes (views) were projected on the lens of the camera that were xz-plane, which was directly from the box to the lens of the camera and yz-plane, which was the reflection of the bubble into the mirror. A schematic diagram of the test section is shown in Fig. 1.

Because of the use of the mirror, two light sources were used to illuminate the area of recording for both the camera and the mirror. A light diffuser was also placed between each light source and the box to ensure the even distribution of the light inside the box and the mirror views. It is important in the experiment to balance the light sources for the bubble in the column and the mirror because sometimes the light is scattered from the bubble surface while it is wobbling particularly for the projection of the bubble in the direct view.

The bubbles were allowed to rise freely beyond control environment (controlled experiments) in order to mimic the real industrial situation regarding getting two bubbles with different sizes. As a result, the equivalent radii of the bubbles produced deviated at most by 10%. The bubbles are also accordingly produced having different initial configurations: an offset in both vertical and horizontal directions, $0^\circ < \theta < 90^\circ$; and sometimes they rise side by side, $\theta = 0^\circ$.

Bubble pairs were recorded using a high-speed video camera (NAC HotShot) running at 500 frames per second. The water level was 200 mm above the tip of the nozzles. The field of view was a less than this with a height of 180 mm which equivalent to a spatial resolution of 0.148 mm/pixel. With reference to Fig. 2, the non-dimensionalised initial axial separations, $\Delta x/r_{ave}$, normalised by the average bubble radius, $r_{ave} = 0.5(r_1 + r_2)$, were 4 and 4.5 and a considerable number of measurements were collected (over 200 data points for each nozzle gap). This provides a significant database to generate bubble-bubble interaction statistics. Bubble pairs that rise at an offset were isolated and then placed into different categories depending on their initial non-dimensionalised vertical separation distance, $\Delta z/r_{ave}$. Based on that, the non-dimensionalised centre-to- centre separation distance,

$$s = \frac{2\sqrt{\Delta x^2 + \Delta z^2}}{r_1 + r_2}, \tag{1}$$

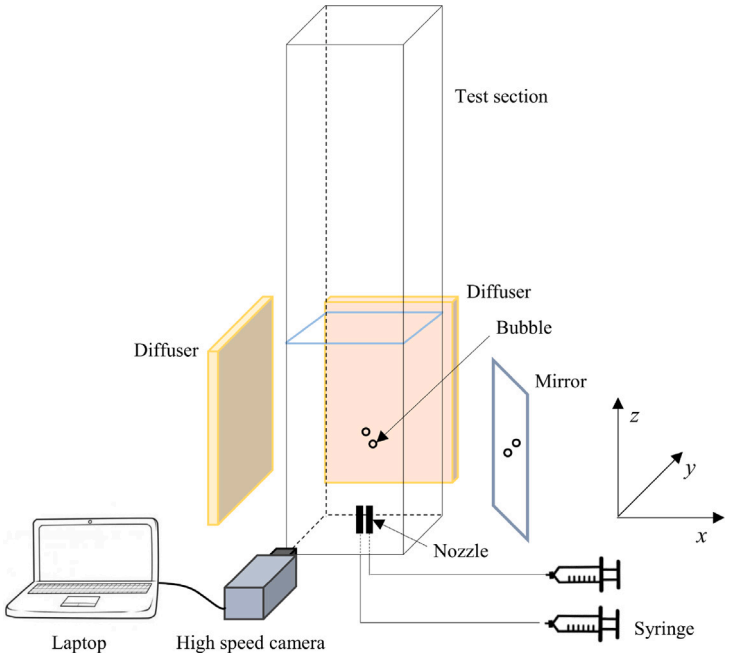

Fig. 1. Schematic of the experimental apparatus.

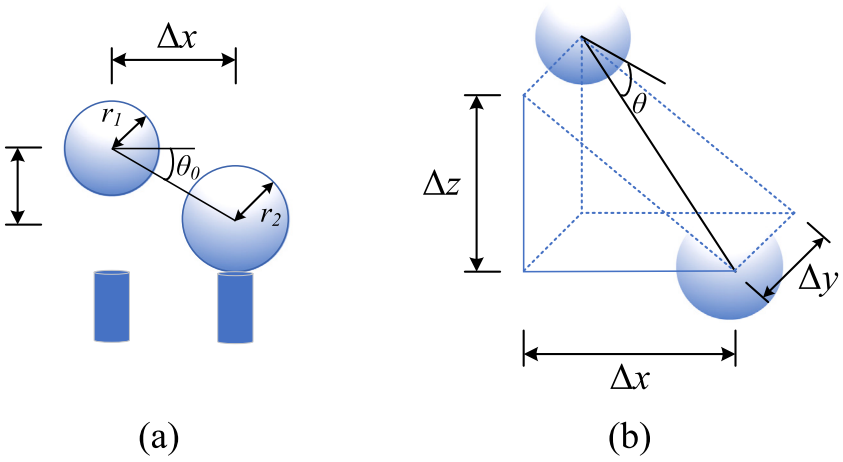

Fig. 2. Schematics of (a) the initial release of the bubbles and (b) the more general case of the bubbles rising.

lies in the range of $4.2 < s < 11$. Similarly, the initial relative angle,

$$\theta_i = \tan^{-1}\left(\frac{\Delta z}{\Delta x}\right), \tag{2}$$

was in the range $20° < \theta_i < 65°$. Finally, we define the average Reynolds number

$$\mathrm{Re}_{\mathrm{ave}} = \frac{\rho_l\left(|w_1 r_1| + |w_2 r_2|\right)}{\mu_l}, \tag{3}$$

where ρ_l and μ_l are the density and dynamic viscosity of the water and w_i is the z-component of the rise velocity of the ith bubble.

In order to gather this detailed positional and kinematic information, the transient behaviour of the bubbles was analysed using the image processing libraries in MATLAB. The identification of the bubbles in the captured images is carried out by subtracting each frame, Fig. 3(a), from a background frame, Fig. 3b, which is selected when both bubbles are completely outside the field of view. RGB images are converted to grey-scale images. A global threshold is applied, following the work of Otsu (1979), to "binarize" the greyscale images, Fig. 3(c). Since there are four bubbles (objects) in each frame, they are isolated by assigning the connectivity parameter of each object as MATLAB labels each object with a unique integer value. Various important parameters can be now derived for each object.

In order to calculate the initial size of each bubble, the bubble rises initially with nearly a spherical shape after the release, the images captured immediately after the release were considered. The bubble at that stage is nearly spherical, allowing the estimate of major and minor axes. The length of the major and minor axes will then be averaged to get the bubble diameter. The centre of mass and the area of each bubble are also extracted at this point.

2.2. Numerical methods

All the computations implemented here were done by solving the governing equations for compressible, laminar Newtonian flow (Keshavarzi et al., 2014; Xie et al., 2014), which are the continuity equation

$$\frac{\partial \rho}{\partial t} + \nabla.(\rho \mathbf{U}) = 0, \tag{4}$$

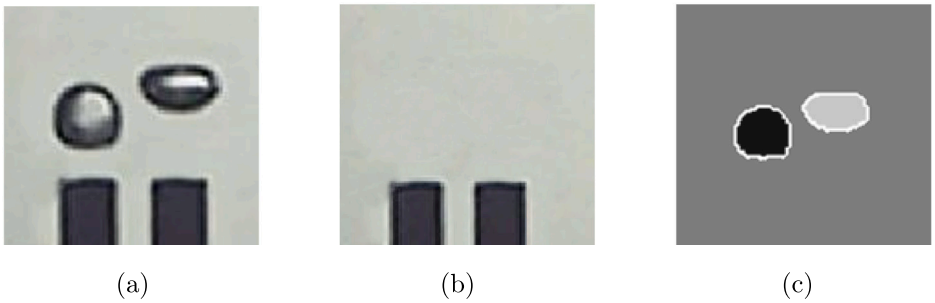

Fig. 3. Detection and binarization of pair of bubbles (a) raw image, (b) global background, (c) binarized image.

and the conservation of momentum

$$\frac{\partial \rho \mathbf{U}}{\partial t} + (\mathbf{U}.\nabla)\,\rho\mathbf{U} = -\nabla P + \mu\nabla^2\mathbf{U} + \rho g + F_\sigma, \tag{5}$$

where $\mathbf{U}$, P, ρ, μ and F_σ are the velocity, pressure, density, dynamic viscosity and surface tension force, respectively. Since we have two-phase flow, the Volume of Fluid (VOF) model is used where an additional equation for the volume fraction of water, α_l, is solved

$$\frac{\partial \alpha_l}{\partial t} + \nabla.\left(\alpha_l \mathbf{U}\right) = 0. \tag{6}$$

If $\alpha_l = 1$, this defines that cell is filled with the liquid phase and if $\alpha_l = 0$, this indicates that the cell has only gas phase inside. A value somewhere between 0 and 1 defines that the cell will have both phases. The source term F_σ in Eq. (5) is calculated using the Continuum Surface Force model (CSF) (Brackbill et al., 1992)

$$F_\sigma = \sigma k \nabla \alpha_l \tag{7}$$

where σ is the surface tension, k is the surface curvature which can be calculated by

$$k = \frac{1}{\mathbf{n}}\left[\frac{\mathbf{n}}{|\,\mathbf{n}\,|}\nabla\,|\,\mathbf{n}\,| - \nabla\mathbf{n}\right], \tag{8}$$

where $\mathbf{n}$ is the surface normal at the interface.

We believe that the consideration of the compressibility effects is necessary. That is because the bubble is rising through a hydrostatic pressure gradient and will expand as it rises and this condition is also more realistic at the interface between the phases and the nearby regions. This requires an appropriate equation of state for the gas phase only to be used, which is here the ideal gas equation

$$\rho_g = \frac{P_0 + P}{\frac{R}{M_w}T} \tag{9}$$

where P_0 is the operating pressure, R is universal gas constant, M_w is the molecular weight and T is the temperature. The temperature is constant as isothermal system was assumed in our computations. Thus, there is no need to solve the energy equation.

The viscosity and the density of the mixture in each control volume are averaged depending on the following relations:

$$\rho = (1-\alpha_l)\rho_g + \alpha_l\rho_l, \tag{10}$$

and

$$\mu = (1-\alpha_l)\mu_g + \alpha_l\mu_l, \tag{11}$$

where ρ_g, ρ_l, μ_g and μ_l are the gas and liquid densities and the gas and liquid dynamic viscosities respectively.

All the numerical analyses are performed using ANSYS-Fluent, version 15, in a 3D dimensional domain which is a rectangular box with the dimensions of $0.06\times0.06\times0.22$ m. The water level inside the domain was maintained at 0.2 m, giving a small air-filled space for the bubbles to emerge into. The Navier–Stokes equations are discretised using the Finite Volume Method (FVM). The SIMPLE algorithm is used to couple the pressure with the velocity. Geo-Reconstruct is used as the volume

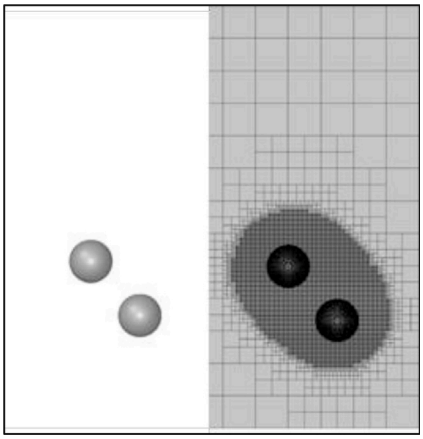

Fig. 4. Left: An isosurface of water volume fraction, indicating the surface of the bubbles; right: The refined mesh region around the two bubbles.

fraction capturing scheme, which gives a sharp interface, not smeared like many other interface reconstruction techniques give. The Geo-Reconstruct method is explicit and so the Courant number is kept, for all the cases, less than 1, necessitating very small time steps. Some initial and boundary conditions were made to simplify the calculations. A rectangular box is filled with stagnant water, by setting the value of α_l to 1 throughout the domain, apart from the aforementioned small air gap above the water and below the top of the domain. Two round bubbles of equal or different sizes at rest are placed at different horizontal and vertical distances from each other near the bottom of the domain. This was done by marking those cells inside the bubble and setting α_l to zero there. The velocity gradient at the walls is included by setting up no-slip boundary condition. A pressure outlet was set at the top of the domain to allow air flow in and out of the domain as the bubbles expanded during their rise.

The computational cost of using a fixed mesh resolution throughout the domain that was capable of resolving the bubbles and their coalescence was too high. A new adaptive meshing technique was developed that utilises the existing mesh refinement and coarsening features of ANSYS-Fluent. Here, a Lagrangian equation is solved using the User-Defined Scalar (UDS) feature in ANSYS-Fluent

$$-\frac{\partial}{\partial x_i}\left(\Gamma\frac{\partial \phi}{\partial x_i}\right) = S_\phi, \tag{12}$$

where ϕ is some scalar, Γ is the diffusion coefficient and S_ϕ is a source term – the advective term in the UDS was set to zero. Through a User-Defined Function (UDF), S_ϕ is set to +1 wherever in the domain $\alpha_l > 0.5$ and at the walls of the domain ϕ is fixed at zero. Once the UDS is solved, at each timestep, wherever in the domain the value of ϕ is greater than one quarter of its maximum value in the domain, a User-Defined Memory (UDM) is set equal to one, elsewhere it is zero. This effective marks are region of the mesh that contains the bubbles and a

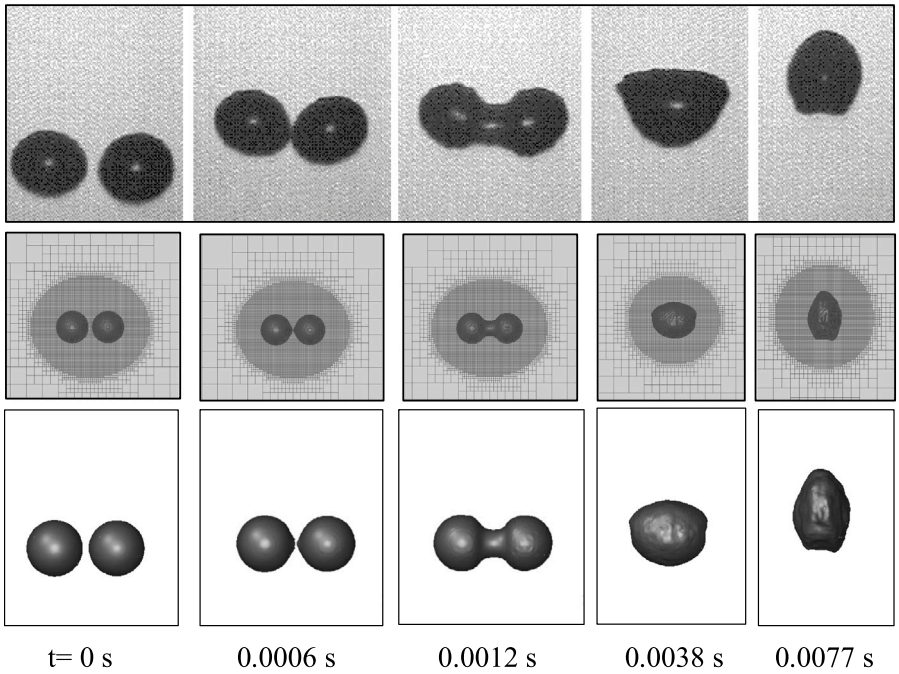

Fig. 5. The comparison of our adaptive mesh technique (second and third rows) with the experiments of Duineveld (1998) (first row). The simulation results agree well with the experiments, thus validating the numerical model.

significant volume around them besides. Cells inside this marked region are refined, while those outside are progressive coarsened back to the background refinement. In this way, a "halo" of refined cells follows the bubbles as they rise through the domain, as can be seen from Fig. 4.

2.2.1. Numerical model verification

Our adaptive mesh is validated here against the experiments of Duineveld (1998) for the coalescence of two air bubbles rising side by side in water. The radius of each bubble is r = 0.9 mm and the dimensionless separation distance, s, between them is 2.22. Fine mesh was used to simulate the coalescence whereas each bubbles had 15 cells per radius. The coalescence process is depicted in Fig. 5 in comparison with the experiments. This figure shows that the numerical results of our adaptive mesh model agree well the experiments of Duineveld (1998). In addition, it shows the robustness of the numerical model in capturing the curvature and topology of the coalesced bubbles during the different stages of coalescence that are vapor bridging, horizontal and vertical shrinking and bullet-like bubble. The second row of the figure shows the adaptive region enclosing the rising bubbles and the change in its size and shape before and after the coalescence. This will result in a reduction in the total number of cells required for the simulation. Hence, the effectiveness of our adaptive meshing in reducing the computational cost was tested through a comparison over the total number of cells required for capturing the coalescence for fixed and adaptive meshes. Two identical bubbles with radii of 2 mm were allowed to rise freely side by side in a 3d computational domain of (15 × 15 ×180 mm). For the fixed mesh, a huge number of cells is required which is around 49 million cells to cater for the coalescence process. While, the adaptive meshing technique requires only 630 000 cell as initial gridding to achieve similar resolution, 22 cells per radius, that was used with the fixed mesh case.

3. Interaction of bubble pairs at small separation distances

In this section, we will try to highlight and address the different factors that affect the coalescence of bubbles. For that purpose, the collected experimental data will be analysed. Accordingly, the numerical modelling will be set depending on these factors in the next section. This would really help for better understanding of that complex process and therefore its modelling can be improved.

3.1. Effect of separation distance on coalescence of bubbles

Since the bubbles were released at small axial separation distances, many coalescence events were recorded. The coalescence probability data was correlated with the vertical separation distance, Δz, for all the axial separation distances, Δx, used as can be seen in Fig. 6. At $0 < \Delta z < 0.5$ the bubbles were considered to coalesce at side by side mode, $0° < \theta < 10°$.

First of all, the probability of coalescence when the bubbles rose side by side was at its highest value, 0.35, for the smallest axial separation distance, $\Delta x = 2.25$. In comparison to the other two axial separation distances studied $\Delta x = 2.375$ and $\Delta x = 2.5$, the coalescence probability has generally decreased to 0.26 and 0.2 respectively.

Then, the probability of coalescence was significantly decreased as the relative angle, θ_i, slightly deviated from 0°. This sudden decrease was observed when the bubbles, for all the axial separations, were vertically separated by a distance approaches to 1. A probable reason for that is that the effect of the vorticity of the leading bubble wake is significant at that distance. The vorticity here acts as a drift force (lift force) on the trailing bubble as was proposed by the analytical and numerical studies of Harper (1997), Hallez and Legendre (2011). This could result in the trailing bubble being quickly pushed away from the effective region of attraction of the leading bubble and therefore the chance of coalescence would be decreased. Although this scenario was reported for the spherical bubbles, this can be considered valid here for the ellipsoidal bubbles studied based on the decreased probability of coalescence observed. However, for the ellipsoidal bubbles, another scenario is expected where even if the trailing bubble is initially drifted from the line of the interaction, it would rejoin again due to the lateral migration nature of both ellipsoidal bubbles. A velocity contours map from the simulation is depicted in Fig. 7 showing these expected scenarios that a trailing bubble could experience while it rises in the vicinity of the wake of a leading bubble.

An appreciable increase in the coalescence probability was noticeable for the smallest axial gap when the bubbles were within a vertical distance, Δz close to 1.5. That was followed by a remarkable increase, especially for the smallest axial separation distance, Δx, when the bubbles separated by a non dimensional distance equivalent to 2. Here,

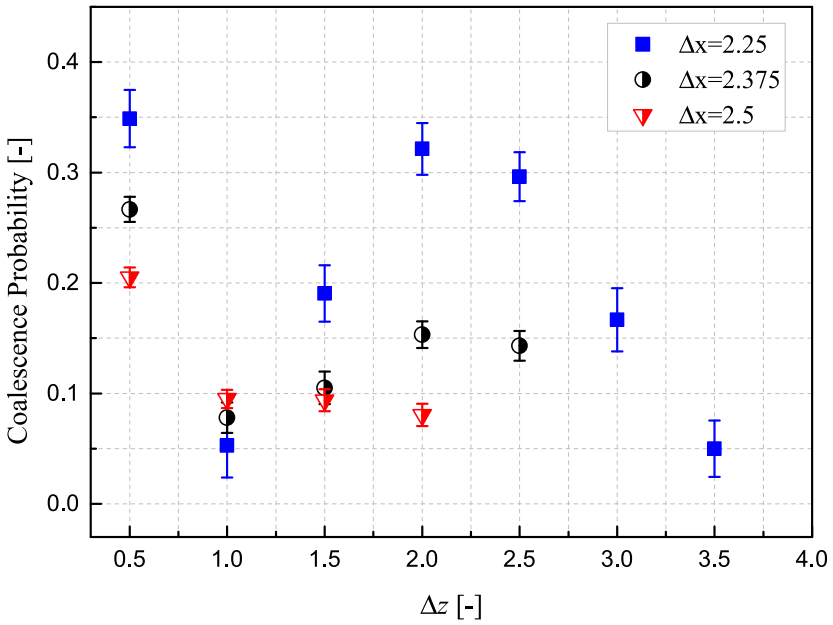

Fig. 6. Coalescence probability from set of the three nozzles used in this study, the error bars represent the standard error which relates the standard deviation to the sample size.

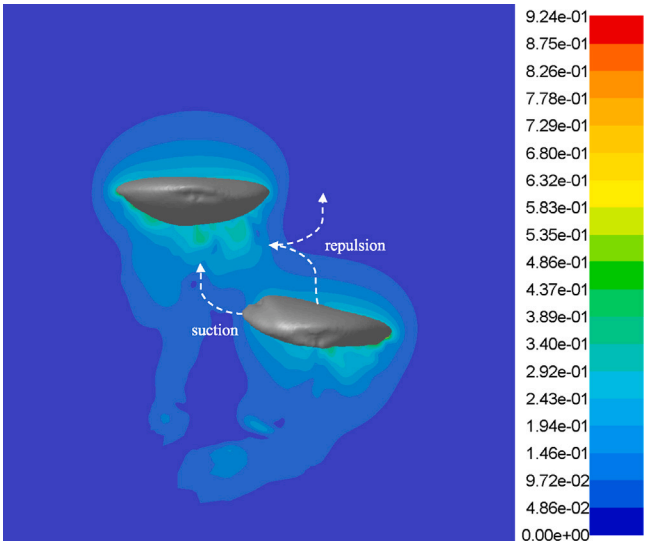

Fig. 7. The expected scenarios that a trailing bubble could experience when it travels nearby the wake of a leading bubble.

the contribution of the vorticity of the leading bubble wake is still effective in drifting the trailing bubble but the difference is that the vertical distance between bubbles is large enough so that the trailing bubble would have approached the leading bubble. The approach could be because the size of the trailing bubble is smaller than the size of the leading bubble. As a result, the trailing bubble has the greater rise velocity which would have made the trailing bubble approaching the leading bubble. Afterwards, a drop down in the tendency of coalescence was gradually seen apart from $\Delta z = 2$.

A similar trend was predicted for the next separation distance $\Delta x = 2.375$. However, after the reduction in the coalescence probability at $\Delta z = 1$, a moderate jump in the coalescence probability was observed compared to that at $\Delta x = 2.25$. The reason here might be owing to the increase in the axial separation distance, Δx, between the bubbles. There were no coalescence events recorded when Δz was larger than 2.5. The behaviour for $\Delta x = 2.5$ showed a different mode of coalescence probability where there was no jump in the behaviour after the reduction at $\Delta z = 1$. The coalescence probability at that distance was even a bit greater than those for $\Delta x = 2.25$ and 2.375. Apart from $\Delta z = 2$, the likelihood of coalescence has dropped down again for all of the gaps. It should be added here that the coalescence was not observed when larger axial separation distance, $\Delta x = 2.62$, was used. The statement can be drawn here that the theoretical studies could be validated by the experiments even though the previous was based on small spherical bubbles.

3.2. Effect of relative bubble size on coalescence of bubbles

It is worth seeking another factor that might contribute to increasing or decreasing the coalescence probability. The radii ratio of the trailing bubble to the leading bubble, r_2/r_1, was plotted against the average Reynolds number, Re_{ave}, of both bubbles. Striking results have been found when the ratio of the bubble sizes decreased below 1, the coalescence probability was highly increased. It was found in most cases that the radius of trailing bubble slightly deviated from that of the leading bubble. The reason for that is the small deviation in the size of the rising bubbles, which in turn influences the rise velocity. These results are plotted in Fig. 8.

Here, it is the trailing bubble has the greater rise velocity which makes the trailing bubble approaching the leading bubble gradually until they row at an angle, $\theta_c \leq 40°$, and then they get coalesced. Similar graph was produced by Kusuno and Sanada (2015a) for spherical bubbles with equal size. Our findings are completely opposite to their findings owing to the different bubble sizes which for our study lie within the ellipsoidal regime. This can be clearly seen from the relationship between the terminal rise velocity and the bubble size of Clift et al. (1978), Fig. 9. This figure indicates that there are three distinct regions, characterised by positive (Region 1), then negative (Region 2) and then positive (Region 3) gradients. In Region 2 on the curve, $0.7 < r < 3.5$ mm, shows that the rise velocity gradient is negative. This means that for a particular size range of bubble, smaller bubbles will rise more rapidly than larger bubbles. An ellipsoidal bubble is no longer spherical and slows down because it develops a secondary motion (lateral motion). Hence, that imposed the trailing bubble (smaller bubble) had the greater average rise velocity compared to that of the leading bubble (larger bubble).

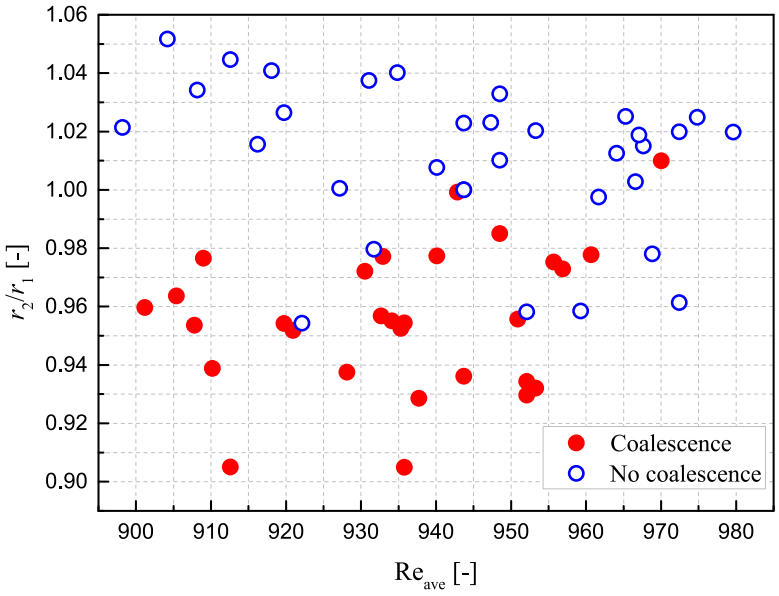

Fig. 8. Effect of relative bubble size on the coalescence of bubbles when the trailing bubble is smaller than the leading bubble, there is a higher probability of coalescence.

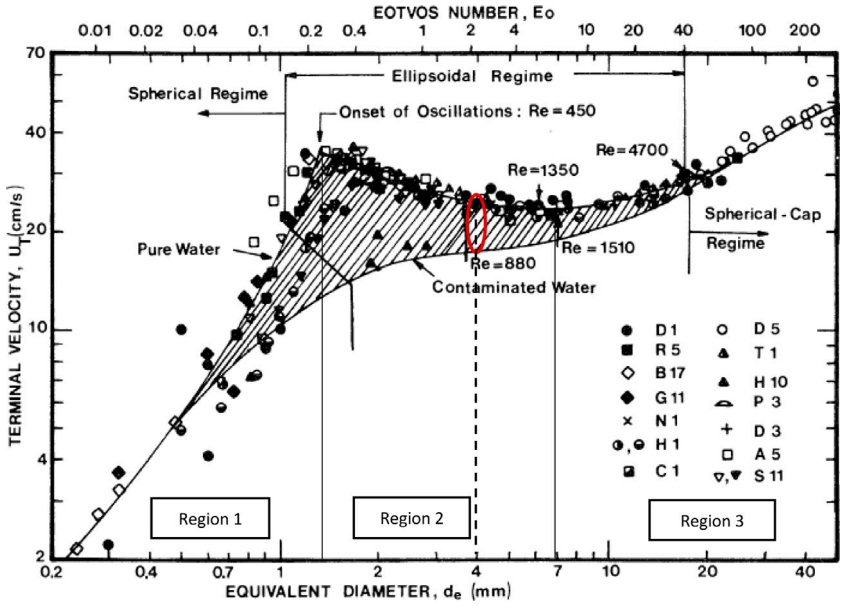

Fig. 9. The rise velocity of air bubbles in water against their equivalent diameter (Clift et al., 1978).

The encouraging finding is that the difference can be effective as it has been found that when the ratio of the trailing bubble size to the leading one is appreciably small, even when $r_2/r_1 \simeq 2.3\%$, the coalescence is more likely to happen. However, if the trailing bubble has equal or larger size, the probability of coalescence of those bubbles is rare. This is explained by the negative gradient in the terminal velocity that an ellipsoidal bubble has when its size is in the ellipsoidal range ($r \approx 0.7$–2.5 mm) as was shown in the general relationship between the terminal rise velocity and the bubble size in Clift et al. (1978). It is also worth mentioning that the data showed in Fig. 8 was captured at a vertical distance, Δz, larger than 2. That is to avoid the eventual deformation of the bubbles that could lead to coalescence although we know the higher contribution of the vorticity of the wake of the leading bubble in preventing the coalescence. The vorticity develops a drift force which would result in the trailing bubble to be quickly pushed away from the leading bubble.

An example of coalesced pairs is presented in Fig. 10. The superimposed images and its corresponding 3D behaviours of the coalesced bubbles are shown in Fig. 10(a) and Fig. 10(b), respectively. Here, the trailing bubble is smaller than the leading bubble by ≈ 5%. The trailing bubble, the smaller bubble, first travelled away from the leading bubble due to the developed drift force from the wake of the leading bubble as it was explained by Hallez and Legendre (2011). Then the bubbles, during their migration around each other, crossed each other and the trailing bubble continued separating from the leading bubble at some places until it reached the leading bubble from the side and merged with it. That was the observation in most of the coalesced data points at offset configurations reported in this study.

While, Fig. 10(c) shows the instantaneous rise velocity of both bubble. This figure shows that the average rise velocity of the trailing bubble, w_2 is greater than that of the leading bubble, w_1, by ≈ 11 mm/s. That slight difference might have drastically contributed to the coalescence process seen in Fig. 8.

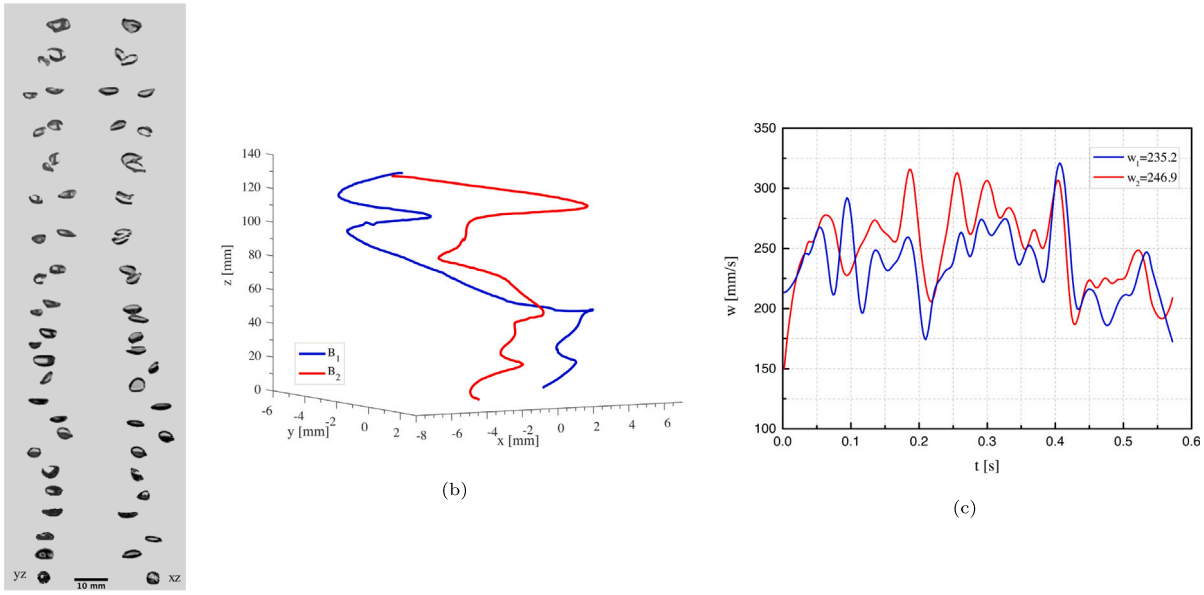

Fig. 10. Relative motion of two coalescing bubbles, the trailing bubble is smaller than the leading bubble by 5% (a) superimposition of frames in xz and yz planes showing the approach of the trailing bubble, (b) 3D trajectory of both bubbles, (c) rise velocity of both bubbles.

Next, the separation distance, s, was plotted against the coalescence angle, θ_c, the angle between the bubbles prior to the coalescence. The relationship is shown in Fig. 11. Here, in the relation between θ_c and s, most of the data showed that the coalescence happened when the trailing bubble approached the leading bubble at $\theta_c \leq 40°$. This is consistent with our observations regarding the approach of the trailing bubble to the leading bubble based on its appreciably greater rise velocity. The contribution of the wake is seen less because the initial separation distance between the bubbles is small so that the trailing bubble would be more affected by the vorticity of the wake that push the trailing bubble away. The slight difference in the velocity of rise of the trailing bubble, also contributes in further decreasing of the distance separating the bubbles. The trailing bubble could return to the effective region of the wake where it can be caught by the wake of the leading bubble and therefore the coalescence happened. This scenario has low probability as it can be seen in Fig. 11. In Fig. 11 also the relative interaction between the bubbles that is represented by the initial angle, θ_i, at the release is correlated against the separation distance, s. This is important to show initial boundaries at which the coalescence is more likely to happen. The bubbles are attracted to each other when they are in the range of $25.5° < \theta_i < 57.6°$. There is no previous study has identified these boundaries except the theoretical work of Kok (1993a) which was for spherical bubbles with equal size using the potential flow theory. He found that the bubbles could coalesce if θ_i between them is $35° < \theta_i < 54.7°$. It seems that the ellipsoidal bubbles in our study do not deviate much from the findings of Kok (1993a) except a small deviation in the smallest angle, $\theta_i = 25.5°$. It should be noted that, at this angle, the coalescence between the bubbles is rare.

It should also be referred to that the slight difference in the size of the rising bubbles could have played an important role in the enhanced probability of coalescence compared to the work of Kok (1993a) which was based on equally sized bubbles. More information on the spatial boundaries of the interaction of the bubbles will be deduced in the next section when validating the numerical simulations against the experiments.

In order to support our observations, a few experiments were conducted by generating a trailing bubble much smaller than the leading bubble. The trailing bubble produced at an equivalent radius equals to $r \approx 1.4$ mm by replacing the nozzle responsible for releasing the trailing bubble with a smaller one. One of the axial separation distance, $\Delta x = 2.25$, studied here was tested. It was selected because it is presenting the highest probability of coalescence. Two examples of coalescence are shown in Fig. 12 which shows the superimposed evolution for the bubbles before and after the coalescence. In the first example in Fig. 12(a), the centre to centre separation distance between the bubbles, s, is 4.7 ($\Delta z = 2.5$). These parameters were normalised by the radius of the leading bubble, r_1. The behaviour of the trailing bubble is interesting here where, in addition to its approach of the leading bubble from the side, it has overtaken the leading bubble which then caught the trailing bubble and merged with it. This behaviour can be considered due to the further increase in the rise velocity of the trailing bubble at this size.

In the second example, Fig. 12(b), the striking conclusion was that the trailing bubble approached the leading one and got coalesced with it at a larger separation distance, $s = 6.9$, which was almost double the distance over which the coalescence occurred when the slight deviation between the bubbles is within 10%. The reason for that is the rise velocity of the trailing bubble becomes much greater than that of the leading bubble which makes it possible for the trailing bubble to approach the leading bubble. It is also worth mentioning that it has been found that the probability of coalescence for these experiments was enhanced where 8 runs out of 20 showed coalescence. A quantification on the coalesced pairs is summarised in Table 1.

Table 1
Summary of coalescence parameters of additional experiments to test the effect of further deviation in bubble size ratio on the coalescence.

Coalescence	r_1 [mm]	r_2 [mm]	r_2/r_1 [–]	s [–]
yes	1.88	1.39	0.74	4.2
yes	1.85	1.41	0.76	6.9
yes	1.86	1.34	0.72	7.7
yes	1.91	1.39	0.73	8.2
yes	1.93	1.62	0.84	5.8
yes	1.86	1.52	0.82	6.4
yes	1.87	1.51	0.81	6.1
yes	1.89	1.49	0.79	6.6

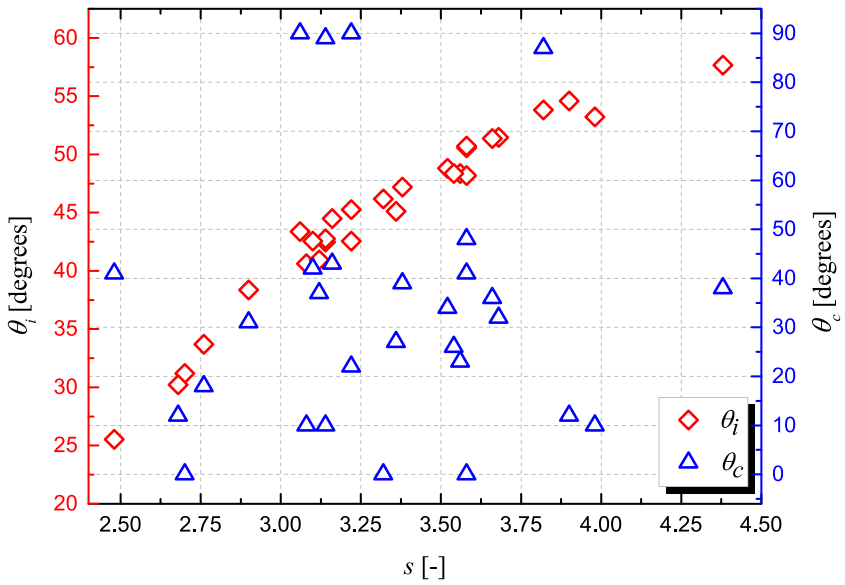

Fig. 11. Initial and final interaction between the bubbles represented by the initial relative angle, θ_i, and the coalescence (equilibrium) angle, θ_c.

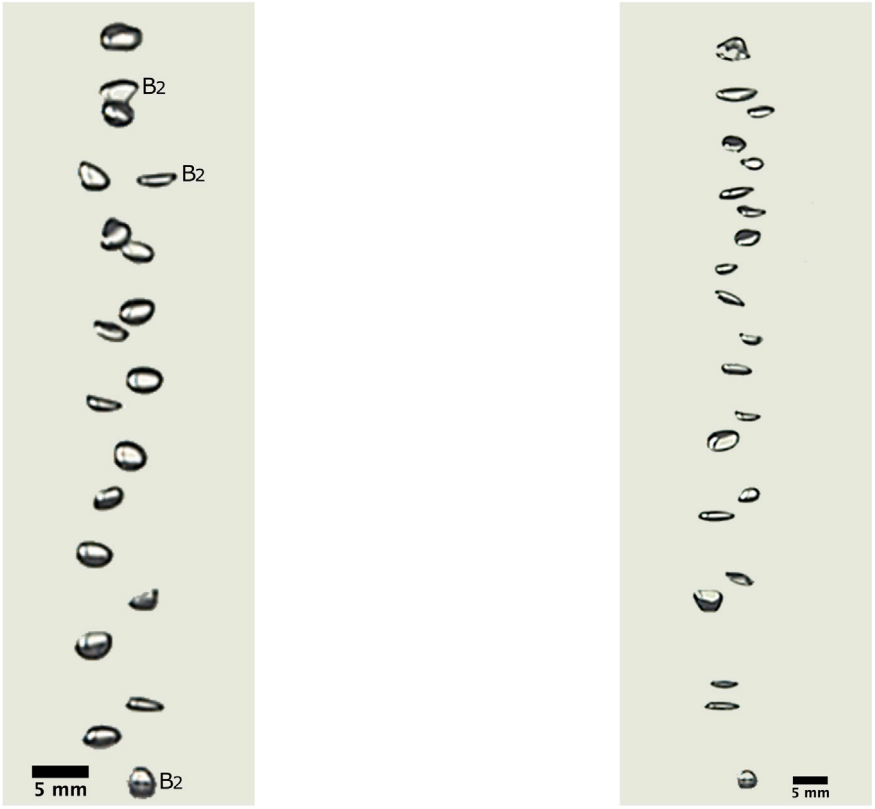

(a) r_1=1.88 mm, r_2=1.39 mm (b) r_1=1.85 mm, r_2=1.41 mm

Fig. 12. Time evolution of the coalescence of two different sized bubbles.

Some of the experimental data that show both coalescence and no coalescence events is tabulated in Table 2. Similar parameters to those presented by Kok (1993b) have been reproduced.

A relationship, which is to the best knowledge of the authors is shown for the first time, has been found when correlating the radii ratio and the time required for coalescence. This relationship, Fig. 13, indicates that the smaller the trailing bubble size is, the less the time required for the coalescence and vice versa.

A general trend could be easily fitted to represent that behaviour even though a few points on the graph deviated from that trend. The deviation from the trend could be ascribed to another factor that is the separation distance, s, between the bubbles which is appreciably

Table 2
Summary of the important parameters of experimental results obtained.

Coal.	r_{ave} [mm]	s [–]	r_2/r_1 [–]	θ_i [deg.]	t_c [ms]	θ_e [deg.]	Coal.	s [–]	r_{ave} [mm]	r_2/r_1 [–]	θ_i [deg.]	t_c [ms]
yes	1.98	3.57	0.985	50.56	726	0	no	3.80	1.97	1.028	53.31	> 800
yes	1.99	3.81	0.975	53.81	658	87	no	4.21	1.96	1.023	57.08	> 800
yes	1.89	3.97	0.963	53.22	528	10	no	3.43	2.02	1.007	49.51	> 800
yes	1.90	3.56	0.938	48.35	472	23	no	3.51	2.02	1.025	50.71	> 800
yes	1.95	3.68	0.928	51.46	414	32	no	3.53	2.05	0.977	51.51	> 800
yes	1.97	3.65	0.936	51.37	468	34	no	3.97	2.03	1.019	55.95	> 800
yes	1.99	3.57	0.932	50.71	340	65	no	3.80	2.03	1.014	54.51	> 800
yes	2.02	3.05	1.00	43.36	556	79	no	4.02	2.03	1.040	56.62	> 800
yes	1.99	3.15	0.972	44.49	607	90	no	3.98	2.01	0.961	55.87	> 800
yes	1.98	3.21	0.934	45.25	546	22	no	3.10	1.98	1.012	43.03	> 800
yes	1.94	3.21	0.972	42.48	584	10	no	2.85	1.97	1.010	36.83	> 800
yes	1.89	3.14	0.976	42.55	610	90	no	3.10	1.92	1.000	41.06	> 800
yes	1.88	3.21	0.959	48.18	484	48	no	3.10	2.00	1.026	43.56	> 800
yes	1.94	3.58	0.977	42.75	646	86	no	2.78	2.03	1.04	37.32	> 800
yes	1.92	3.14	0.951	40.62	514	10	no	2.42	2.03	1.019	24.17	> 800
yes	1.92	3.08	0.954	57.67	454	38	no	2.84	1.99	1.024	37.32	> 800
yes	1.96	4.26	0.999	42.55	314	42	no	3.28	1.98	1.024	46.37	> 800
yes	1.96	3.10	0.974	46.18	714	0	no	3.37	2.02	0.958	48.63	> 800
yes	1.89	3.31	0.953	45.00	496	27	no	3.59	2.01	1.002	51.41	> 800
yes	1.98	3.35	0.929	54.59	622	12	no	3.06	2.02	1.018	43.23	> 800
yes	1.98	3.90	0.955	38.35	496	31	no	3.05	1.97	1.000	41.56	> 800
yes	2.01	2.89	0.977	25.54	534	89	no	3.08	2.00	0.958	43.23	> 800
yes	1.94	2.47	0.956	30.21	524	16	no	3.20	1.94	0.979	43.76	> 800
yes	1.95	2.67	0.904	33.69	332	18	no	3.11	1.92	0.954	41.28	> 800
yes	1.95	2.76	0.954	40.94	502	51	no	3.29	1.88	1.051	43.70	> 800
yes	1.98	3.12	0.955	31.18	456	0	no	3.20	1.93	1.00	43.56	> 800
yes	1.90	3.55	0.905	48.35	340	12	no	3.16	1.99	1.022	44.42	> 800
yes	1.93	3.52	0.937	48.85	402	46	no	3.22	2.01	1.032	46.10	> 800
yes	1.95	3.39	0.952	47.20	476	39	no	2.95	1.94	1.044	38.58	> 800
							no	2.76	1.89	1.021	30.68	> 800

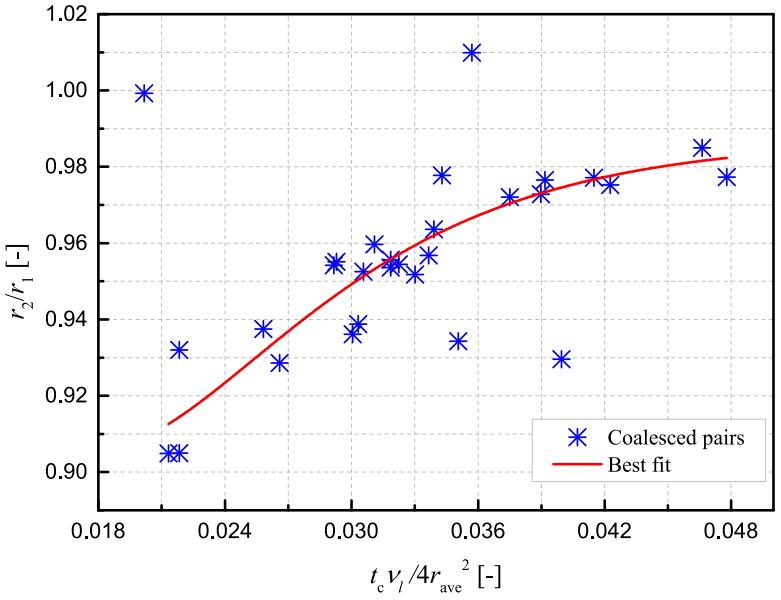

Fig. 13. The nondimensionalised time delay before the coalescence of a pair of bubbles related to the initial bubble size ratio.

deviated at the initial release of the bubbles. However, any small separation distance, s, between the rising bubbles might have been compensated by the greater average rise velocity of the trailing bubble.

For those pairs that did not show the coalescence, however, we are anticipating that the coalescence could be observed between them if the height of liquid in the test section is made larger than that we are investigating in the current paper.

4. Numerical observations

Following the experimental results, we use the numerical simulations to study the effect of the slight deviation in the sizes on the coalescence of air bubbles rising in quiescent water. Here, the computational resources were maximised by selecting spatial resolution between 19.5 and 21.5 per bubble radius, N_r. That was based on the prediction that if the coalescence is likely to happen, the mutual distance between the bubbles should be smaller than the mesh size otherwise the coalescence would occur (Jan, 1994; Bunner and Tryggvason, 2002). This resolution can be considered sufficient to provide accurate tracking for the coalescence of bubbles if it occurs.

The configuration of the bubbles will be restricted between θ_i = 0° (bubbles rising side by side) and θ_i = 90° (bubbles rising in line). Many simulations were carried out using our developed adaptive mesh method to cover different sizes of trailing bubbles and at different

Table 3
Summary of the simulation parameters for the investigated cases.

Case	s [–]	r_1 [mm]	N_r [–]	r_2 [mm]	N_r [–]
a	3.36	2	21.5	2	21.5
b	3.36	2	21.5	1.9	20.5
c	3.36	2	21.5	1.8	19.5

Table 4
Comparison of the parameters obtained from the numerical simulations with the experiments.

Case	Coalescence		Coal. distance [–]		Coal. time t_c [ms]	
	Exp	Sim	Exp	Sim	Exp	Sim
a	No	No	–	–	–	–
b	Yes	Yes	69 r	80 r	568	689
c	Yes	Yes	48 r	67 r	402	596

initial axial separations and centre to centre separations. Those simulations were also used to generalise a map for the boundaries at which the coalescence might occur and in comparison with experiments.

To test the validity of the numerical simulations against the experiments, three cases of simulations representing three different classes of trailing bubble sizes were done. Table 3 lists the simulation parameters and the conditions for the test cases. The conditions for the calculations were set with the following physical parameters: ρ_l=998 kg/m^3, ρ_g=1.225 kg/m^3, μ_l=0.001 N.s/m^2, μ_g=1.8 × 10^{-5} N.s/m^2 and σ=0.072 N/m.

All the bubbles in the simulation runs were initially placed having an axial separation, Δx, and centre to centre separations, s, 2.25 and 3.28, respectively.

Fig. 14 shows the time evolution of the bubbles having three classes of bubble sizes. The case in Fig. 14a shows that the equal bubbles did not coalesce. The bubbles have maintained a constant distance between each other rather than approaching each other. However, the other two cases in Fig. 14b and c have shown coalescence when the trailing bubble size was smaller by 5% and 10% respectively of that of the leading bubble. This agreed well with the experimental findings in the previous section. Another aspect that can be observed from these simulations is the mode of coalescence, especially for the cases b and c described in Fig. 14. They showed a difference in terms of the final orientation before the coalescence. When the bubbles deviated at 5% of their initial bubble sizes in Fig. 14b, the coalescence happened at an angle, coalescence angle, θ_c, equal to 25°. For the case in Fig. 14c in which the bubbles deviated at 10%, the trailing bubble approached the leading bubble from the side and united with it. This would reflect the greater acceleration that the smaller trailing bubble in case c had compared to that in case b. It is also an indication that the numerical approaches can detect the appreciable deviation in bubble sizes which is in an agreement with the experimental approaches. Table 4 presents a quantification for the three cases of the numerical simulations discussed in Fig. 14 with the relevant experiments.

The experiments and numerical simulations agreed well when the trailing bubble is smaller than the leading bubble by 5%. However, when the trailing bubble is smaller than the leading bubble by 10%, a discrepancy of about 50% between both approaches is found. This high deviation could be considered due to the difference in release methods of bubbles in both the simulations and the experiments. It could also be the type and size of the mesh used in the simulations. It should be mentioned the nature of coalescence process of deformed bubbles is complex and the experiments showed a scatter for the time of coalescence with the size deviation.

Next, this study contributes to validate the numerical approaches in capturing the coalescence boundaries in comparison with the experiments. Based on this, a map for the disagreement between these boundaries can be generalised to be used as a guide for future work. It also tests the influence of the slight difference in bubble sizes as a whole on the coalescence process of a pair of deformable bubbles in a numerical frame. That was reached benefiting from our adaptive mesh model which facilitated testing many cases. The map was generated with different bubble classes with respect to the trailing bubble size.

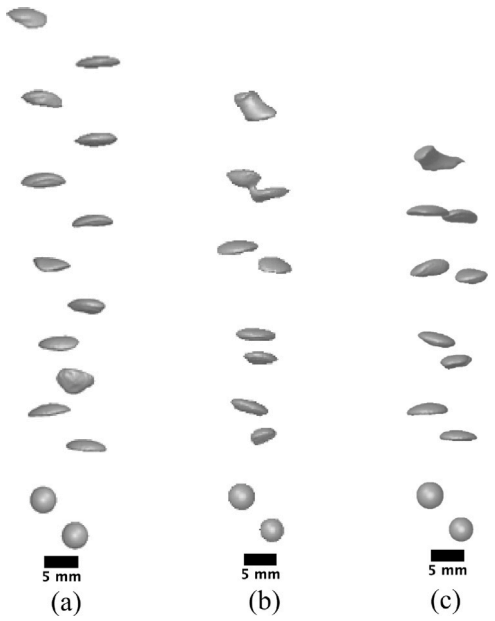

Fig. 14. Tested three cases of deviation in rising bubble sizes (a) equal-sized bubbles, (b) the trailing bubble is smaller by 5% (c) the trailing bubble is smaller by 10%.

The first class was generated when both bubbles have the same initial sizes. The second class of bubbles was when the trailing bubble had a smaller size than that of the leading bubble by 5%. For the separation distances, since the axial distance, Δx, was maintained constant, the separation distance, Δz, was appreciably increased by 0.25 mm for the consecutive simulation runs. Once a bubble pair does not show the coalescence, the separation distance, Δz, is decreased to 0.125 mm between the bubble pair. Then, the simulation run will be repeated depending on the new Δz. Accordingly, 11 simulation runs were needed to generate the map. The coalescence map is shown here at the upmost boundaries at which the coalescence could happen. Then, this map was expressed by the normalised centre to centre separation distance, s, and the initial angle of interaction, θ_i, for a single axial separation distance used in the experiments, Δx = 2.25. This map is shown in Fig. 15.

It has been experimentally shown above that the effect of the deviation in bubble sizes have a high impact on increasing the general tendency of coalescence. Thus, the numerical simulations emphasise the experiments as the unequally-sized bubbles showed coalescence at a distance increased for the axial separation tested. The probability of coalescence when the trailing bubble diameter is smaller by 5% increased by 11% compared to the equally sized bubbles. This probability would increase if the variation in size between rising bubbles is further decreased for instance to about 10%. The map was then produced to relate our maximum experimental boundaries of coalescence compared with simulations. It has clearly shown that the experimental effective region for coalescence is larger than that for the numerical simulations of equal and unequal sized bubbles by 30% and 21%, respectively. This is owing to the difference of initial and boundary conditions between the experiments and the numerical simulations.

Overall, the findings here are of importance as they would improve the detectability of the numerical simulations in any future analysis of complex systems such as bubbly flows.

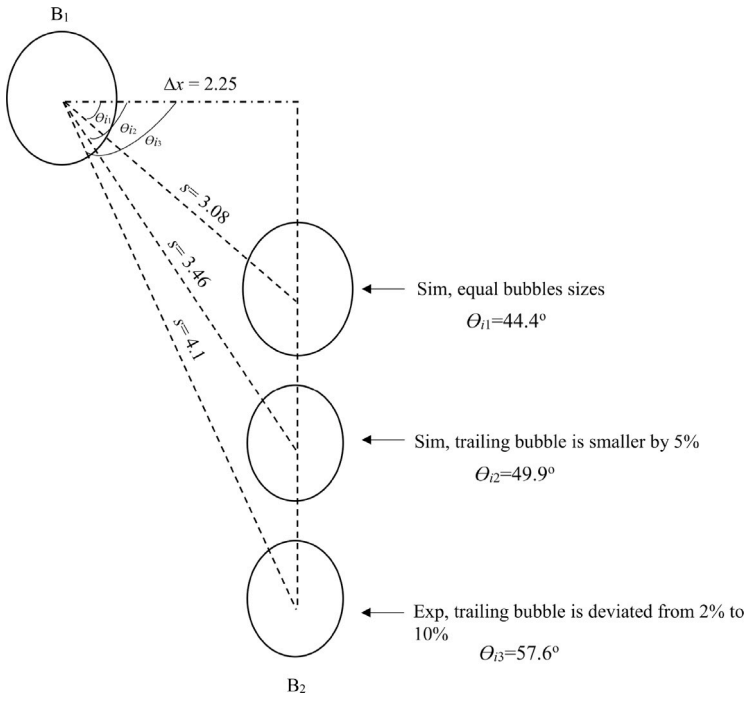

Fig. 15. A map for the spatial boundaries of coalescence from the numerical simulations and the experiments. This map also shows the disparity between both results based on the change in the trailing bubble size.

5. Conclusion

This paper contributed to provide a framework for the understanding of the coalescence process of a pair of deformed air bubbles in water. In a quantitative perspective, it has provided an insight about the likelihood of coalescence events that two nozzles generate in a system of different bubble configurations. Qualitatively, the effect of the leading bubble wake on the coalescence was stated and which agreed with the theoretical work reported by others though their work was based on spherical bubbles interaction. Then, the factors that affect the coalescence process were investigated. It has been found that when the trailing bubble was slightly smaller than the leading bubble, an increased number of successful coalesced bubbles was recorded. The reason for that is the velocity of the trailing bubble which is slightly greater than that of the leading bubble of appreciably smaller size. Additionally, the time required for coalescence was generally related to the deviation in radii. The numerical validation for the experiments was tested using the corresponding model for cases of equal and different sized bubbles. It has well predicted the deviation in size ratio on pairwise coalescence of bubbles. Then, the difference between the experiments and the simulations regarding the effective region over which the bubbles might fuse were highlighted. Hence, this paper has introduced a map to show the boundaries at which the coalescence is likely to happen based on both numerical and experimental observations. It is also shows the general disparity between the numerical simulations and the experiments so that it would establish a ground for further progress on bubbly flow modelling.

CRediT authorship contribution statement

Mustapha A. Al-Behadili: Acquisition of data, Analysis and/or interpretation of data, Writing – original draft. **David M. Hargreaves:** Conception and design of study, Analysis and/or interpretation of data, Writing – original draft, Writing – review & editing. **Buddhika N. Hewakandamby:** Conception and design of study, Analysis and/or interpretation of data, Writing – review & editing.

Declaration of competing interest

The authors declare the following financial interests/personal relationships which may be considered as potential competing interests: Mustapha Al-Behadili reports financial support was provided by The Higher Committee for Education Development in Iraq.

Data availability

Data will be made available on request.

Acknowledgement

All authors approved the version of the manuscript to be published. We thank the Higher Committee for Education Development in Iraq (HCED) for the financial support of this work through grant (D-11-1712). We are also grateful for access to the University of Nottingham High Performance Computing Facility.

References

Agrawal, Meenu, Gaurav, Ashish, Karri, Badarinath, Sahu, Kirti Chandra, 2021. An experimental study of two identical air bubbles rising side-by-side in water. Phys. Fluids 33 (3), 032106.

Balla, Mounika, Kavuri, Sivanandan, Tripathi, Manoj Kumar, Sahu, Kirti Chandra, Govindarajan, Rama, 2020. Effect of viscosity and density ratios on two drops rising side by side. Phys. Rev. Fluids 5 (1), 013601.

Balla, Mounika, Tripathi, Manoj Kumar, Matar, Omar K, Sahu, Kirti Chandra, 2021. Interaction of two non-coalescing bubbles rising in a non-isothermal self-rewetting fluid. Eur. J. Mech. B Fluids 87, 103–112.

Baz-Rodríguez, Sergio A, Ramírez-Muñoz, Jorge, Soria, Alberto, Sacramento-Rivero, Julio C, 2014. Hydrodynamic interaction of two spherical bubbles rising in-line: A semi-analytical approach. Chem. Eng. Commun. 201 (5), 674–687.

Biesheuvel, A., Van Wijngaarden, L., 1982. The motion of pairs of gas bubbles in a perfect liquid. J. Eng. Math. 16 (4), 349–365.

Brackbill, J.U., Kothe, Douglas B., Zemach, Charles, 1992. A continuum method for modeling surface tension. J. Comput. Phys. 100 (2), 335–354.

Bunner, Bernard, Tryggvason, Grétar, 2002. Dynamics of homogeneous bubbly flows Part 1. Rise velocity and microstructure of the bubbles. J. Fluid Mech. 466, 17–52.

Clift, R., Grace, J.R., Weber, M.E., 1978. Bubbles, Drops and Particles. Academic, New York, pp. 181–202.

Duineveld, P.C., 1995. Bouncing and coalescence of two bubbles in pure water. In: IUTAM Symposium on Waves in Liquid/Gas and Liquid/Vapour Two-Phase Systems. Springer, pp. 151–160.

Duineveld, P.C., 1998. Bouncing and coalescence of bubble pairs rising at high Reynolds number in pure water or aqueous surfactant solutions. In: Fascination of Fluid Dynamics. Springer, pp. 409–439.

Hallez, Yannick, Legendre, Dominique, 2011. Interaction between two spherical bubbles rising in a viscous liquid. J. Fluid Mech. 673, 406–431.

Harper, J.F., 1970. On bubbles rising in line at large Reynolds numbers. J. Fluid Mech. 41 (04), 751–758.

Harper, John Frederic, 1997. Bubbles rising in line: why is the first approximation so bad? J. Fluid Mech. 351, 289–300.

Jan, Yi-Jou, 1994. Computational Studies of Bubble Dynamics. University of Michigan.

Katz, J., Meneveau, C., 1996. Wake-induced relative motion of bubbles rising in line. Int. J. Multiph. Flow 22 (2), 239–258.

Keshavarzi, Gholamreza, Pawell, Ryan S., Barber, Tracie J., Yeoh, Guan H., 2014. Transient analysis of a single rising bubble used for numerical validation for multiphase flow. Chem. Eng. Sci. 112, 25–34.

Kok, J.B.W., 1993a. Dynamics of a pair of gas bubbles moving through liquid. I: Theory. Eur. J. Mech. B 12 (4), 515–540.

Kok, J.B.W., 1993b. Dynamics of a pair bubbles moving through liquid. II: Experiment. Eur. J. Mech. B 12 (4), 541–560.

Kumaran, V., Koch, Donald L., 1993a. The effect of hydrodynamic interactions on the average properties of a bidisperse suspension of high Reynolds number, low Weber number bubbles. Phys. Fluids A:(1989-1993) 5 (5), 1123–1134.

Kumaran, V., Koch, Donald L., 1993b. The rate of coalescence in a suspension of high Reynolds number, low Weber number bubbles. Phys. Fluids A:(1989-1993) 5 (5), 1135–1140.

Kusuno, Hiroaki, Sanada, Toshiyoki, 2015a. Experimental investigation of the motion of a pair of bubbles at intermediate Reynolds numbers. Multiph. Sci. Technol. 27 (1).

Kusuno, Hiroaki, Sanada, Toshiyuki, 2015b. Influence of surfactants on the motion of a pair of bubbles in quiescent liquids. Jpn. J. Multiph. Flow 29 (5), 515–522.

Legendre, Dominique, Magnaudet, Jacques, Mougin, Guillaume, 2003. Hydrodynamic interactions between two spherical bubbles rising side by side in a viscous liquid. J. Fluid Mech. 497, 133–166.

Lehr, F., Millies, M., Mewes, D., 2002. Bubble-size distributions and flow fields in bubble columns. AIChE J. 48 (11), 2426–2443.

Lunde, K., Perkins, R., 1998. Shape oscillations of rising bubbles. Appl. Sci. Res. 58, 387–408.

Magnaudet, Jacques, Eames, I., 2000. The motion of high-Reynolds-number bubbles in inhomogeneous flows. Annu. Rev. Fluid Mech. 32 (1), 659–708.

Moore, D.W., 1963. The boundary layer on a spherical gas bubble. J. Fluid Mech. 16 (02), 161–176.

Otsu, Nobuyuki, 1979. A threshold selection method from gray-level histograms. Automatica 11 (285–296), 23–27.

Ruzicka, M.C., 2000. On bubbles rising in line. Int. J. Multiph. Flow 26 (7), 1141–1181.

Sanada, Toshiyuki, Sato, Ayaka, Shirota, Minori, Watanabe, Masao, 2009. Motion and coalescence of a pair of bubbles rising side by side. Chem. Eng. Sci. 64 (11), 2659–2671.

Van Wijngaarden, L., 1993. The mean rise velocity of pairwise-interacting bubbles in liquid. J. Fluid Mech. 251, 55–78.

Van Wijngaarden, Leen, 2005. Bubble velocities induced by trailing vortices behind neighbours. J. Fluid Mech. 541, 203–230.

Watanabe, Masao, Sanada, Toshiyuki, 2006. In-line motion of a pair of bubbles in a viscous liquid. JSME Int. J. Ser. B 49 (2), 410–418.

Xie, Zhihua, Pavlidis, Dimitrios, Percival, James R., Gomes, Jefferson L.M.A., Pain, Christopher C., Matar, Omar K., 2014. Adaptive unstructured mesh modelling of multiphase flows. Int. J. Multiph. Flow. 67, 104–110.

Yuan, H., Prosperetti, A., 1994. On the in-line motion of two spherical bubbles in a viscous fluid. J. Fluid Mech. 278, 325–349.

Zhao, Panpan, Hu, Zhiheng, Cheng, Ping, Huang, Rongzong, Gong, Shuai, 2022. Coalescence-induced bubble departure: Effects of dynamic contact angles. Langmuir 38 (34), 10558–10567.